ACS APPLIED MATERIALS & INTERFACES

www.acsami.org

Research Article

Biocompatible Perovskite Nanocrystals with Enhanced Stability for White Light-Emitting Diodes

Rui Zhang,* Ao Yan, Haiyun Liu, Zehua Lv, Mengqing Hong, Zhenxing Qin, Weijie Ren, Zhaoyi Jiang, Mingkai Li, Johnny C. Ho, and Pengfei Guo*

Cite This: *ACS Appl. Mater. Interfaces* 2024, 16, 34167−34180

Read Online

ACCESS | Metrics & More | Article Recommendations | Supporting Information

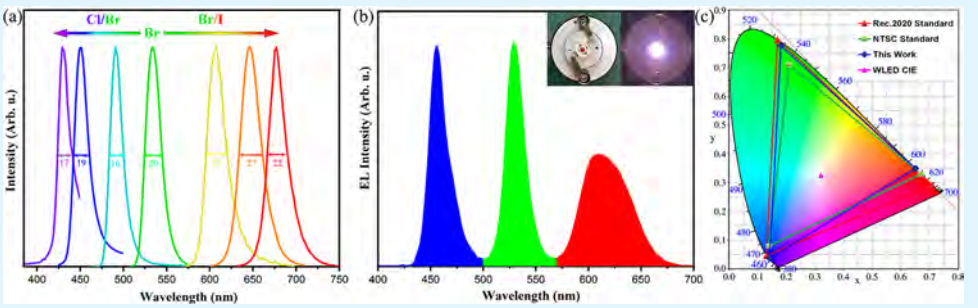

ABSTRACT: Recently emerged lead halide perovskite $CsPbX_3$ (X = Cl, Br, and I) nanocrystals (PNCs) have attracted tremendous attention due to their excellent optical properties. However, the poor water stability, unsatisfactory luminescence efficiency, disappointing lead leakage, and toxicity have restricted their practical applications in photoelectronics and biomedical fields. Herein, a controllable encapsulated strategy is investigated to realize $CsPbX_3$ PNCs/PVP @PMMA composites with superior luminescence properties and excellent biocompatibility. Additionally, the synthesized $CsPbBr_3$ and $CsPbBr_{0.6}I_{2.4}$ PNCs/PVP@PMMA structures exhibit green and red emissions with a maximal photoluminescence quantum yield (PLQY) of about 70.24% and 98.26%, respectively. These $CsPbX_3$ PNCs/PVP@PMMA structures show high emission efficiency, excellent stability after water storage for 18 months, and low cytotoxicity at the PNC concentration at 500 $\mu g\ mL^{-1}$. Moreover, white light-emitting diode (WLED) devices based on mixtures of $CsPbBr_3$ and $CsPbBr_{0.6}I_{2.4}$ PNCs/PVP@PMMA perovskite structures are investigated, which exhibit excellent warm-white light emissions at room temperature. A flexible manipulation method is used to fabricate the white light emitters based on these perovskite composites, providing a fantastic platform for fabricating solid-state white light sources and full-color displays.

KEYWORDS: *lead halide perovskites, perovskite nanocrystals, excellent stability, superior biocompatible, white light-emitting diodes*

INTRODUCTION

Lead halide perovskite $CsPbX_3$ (X = Cl, Br, and I) nanocrystals (PNCs) have attracted tremendous research interest owing to their outstanding photoelectronic and photophysical properties, including high light-absorption coefficient, broad fluorescence tunability, high photoluminescence quantum yield (PLQY), narrow full width at half-maximum (fwhm), and high defect tolerance.[1,2] PNCs with narrow emission peaks and high luminescent properties have the potential to be used in high-resolution bioimaging and high-color rendering white light sources.[3] However, the anion exchange usually occurs between PNCs with different halide compositions in colloidal solutions.[4] Also, the leakage of Pb^{2+} ions severely restricts their applications and development in the optoelectronic and biological fields. Moreover, the PNCs are easily degraded in atmospheric environments by moisture, oxygen, or light owing to the low formation energy and ionic properties,[5,6] which hinders their biological applications in cellular imaging. Therefore, developing an efficient strategy to improve water stability and block the lead leakage of perovskite structures is urgently needed for potential applications in cellular imaging[7,8] and light-emitting devices.[9−11]

A great deal of effort and strategies have been devoted to upgrading the stability of PNCs to meet the requirements of practical applications, including (i) modification of the perovskite crystal structure by doping with other external ions based on Goldsmith's theory of tolerance factor, (ii) modification of the surface ligand molecules of the PNCs to enhance the ligand bindings and minimize the ligand loss,[12] and (iii) encapsulation of PNCs into protective layers to prevent the invasion of external molecules.[13−15] The

Received: April 28, 2024
Revised: May 29, 2024
Accepted: June 12, 2024
Published: June 19, 2024

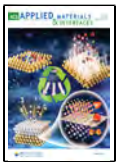

https://doi.org/10.1021/acsami.4c06854
ACS Appl. Mater. Interfaces 2024, 16, 34167−34180

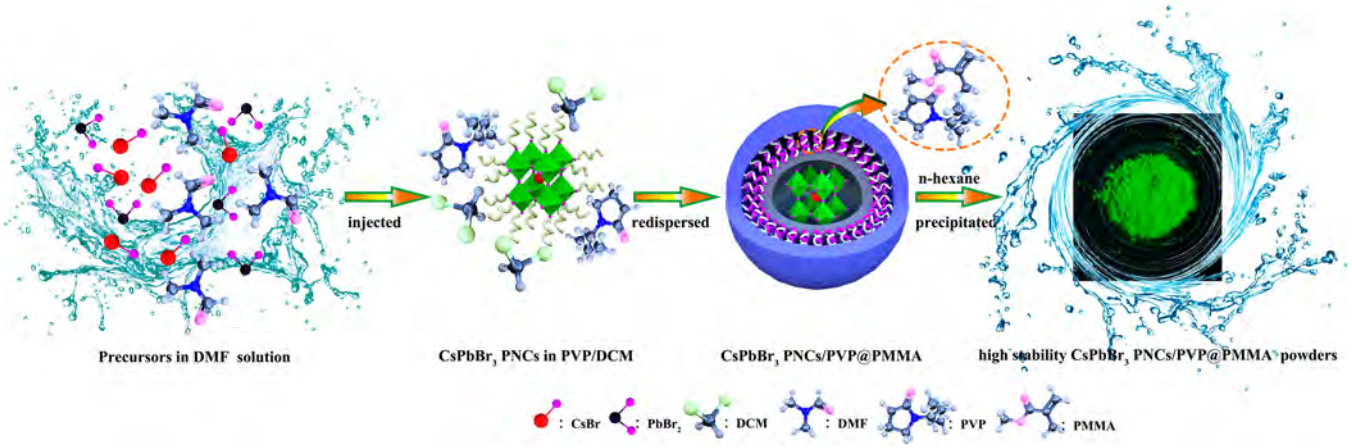

Figure 1. Flow diagram of the $CsPbX_3$ PNCs/PVP@PMMA structure prepared by the core-interfacial layer-shell structures. The middle panel exhibits a schematic drawing of a $CsPbX_3$ PNCs/PVP@PMMA structure after encapsulation.

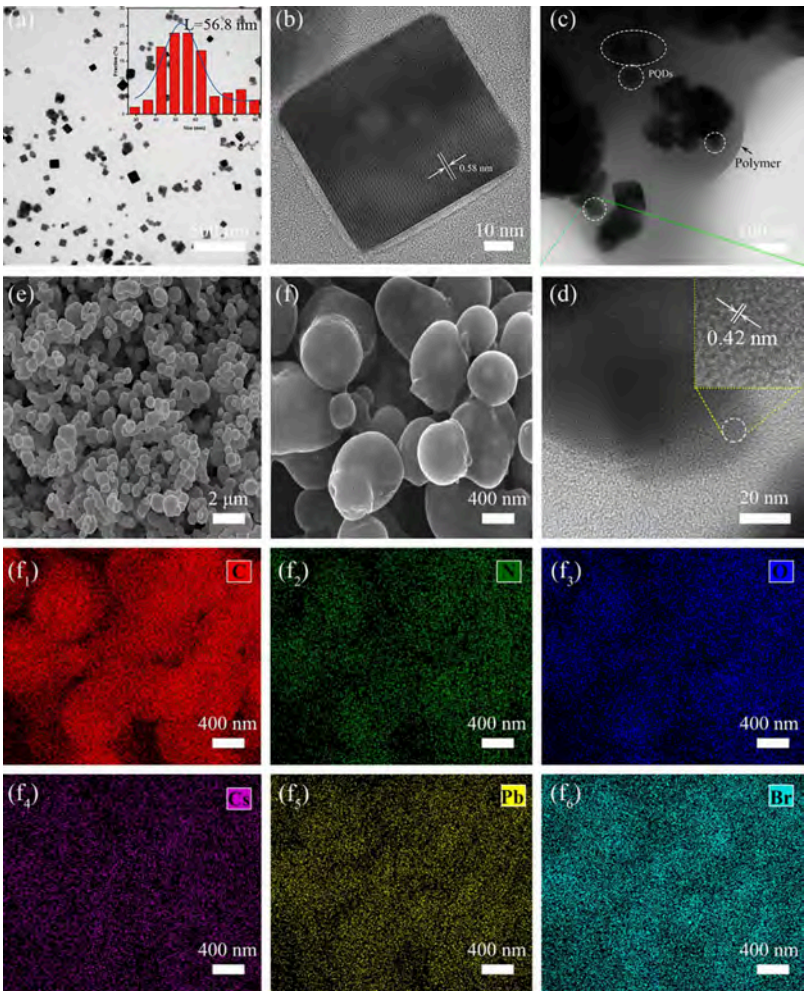

Figure 2. Structural characterization of the $CsPbBr_3$ PNCs/PVP@PMMA composites. (a) Low-resolution TEM image of the $CsPbBr_3$ PNCs/PVP@PMMA structures. Inset shows the average size distribution of PNCs. (b) HR-TEM image of the $CsPbBr_3$ PNCs/PVP@PMMA. (c) Low-resolution TEM image of the $CsPbBr_3$ PNCs/PVP@PMMA powders. (d) HR-TEM images of the $CsPbBr_3$ PNCs/PVP@PMMA powders. (e) Low- and (f) high-resolution SEM images of the $CsPbBr_3$ PNCs/PVP@PMMA powders. (f_1–f_6) Two-dimensional (2D) elemental mapping of the composite powders.

encapsulation methods, as efficient and straightforward methods, show great potential to improve the environmental stability of PNCs. For example, TiO_2,[16−18] AlO_x,[19−21] and SiO_2,[22−25] could be used as the protective layer materials to isolate the PNCs from moisture and oxygen. However, realizing the oxide encapsulation process is still challenging due to time-consuming and uncontrollable hydrolysis reactions, lead leakage, and water molecule erosion.

https://doi.org/10.1021/acsami.4c06854
ACS Appl. Mater. Interfaces 2024, 16, 34167−34180

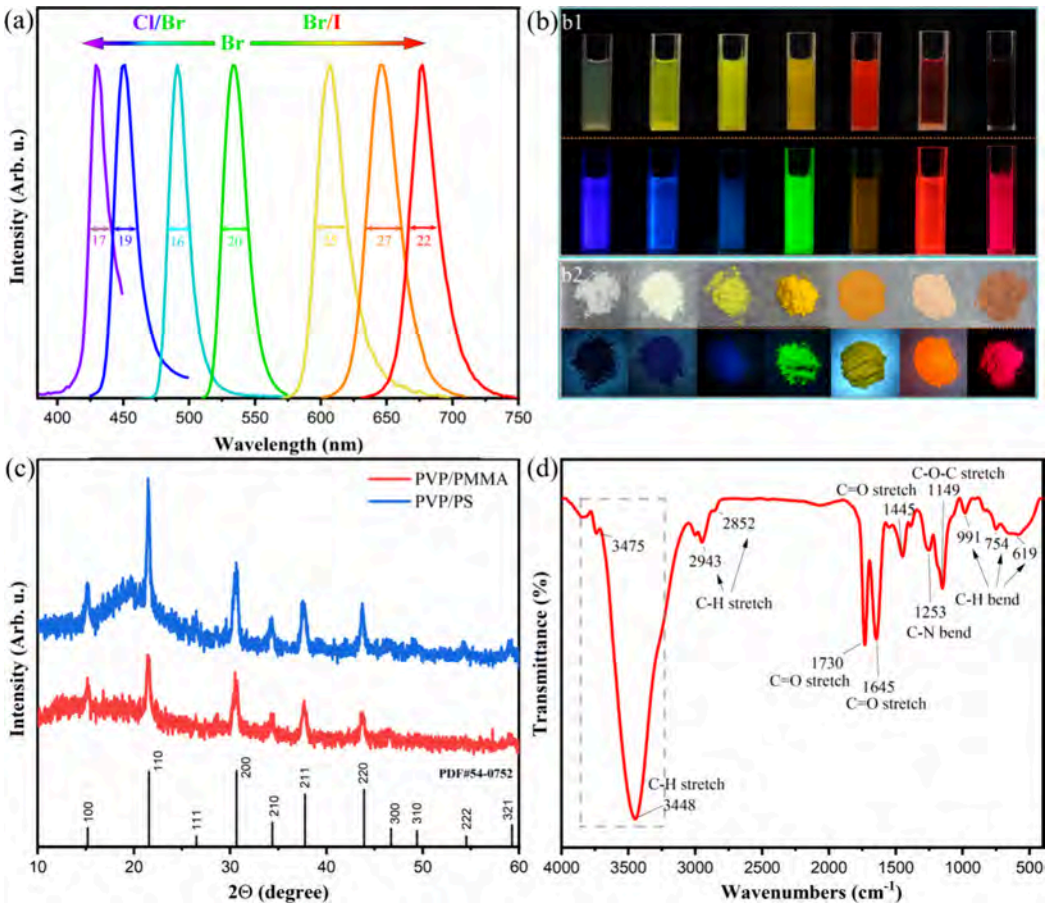

Figure 3. Optical characterization of the composition-tunable colloidal $CsPbX_3$ PNCs/PVP@PMMA structures. (a) PL emission spectra of the tunable composition of lead halide perovskite nanocrystals. (b) Optical photographs of the $CsPbX_3$ PNCs/PVP@PMMA structures and corresponding powders under room light (upper) and a 365 nm UV light illumination (bottom), respectively. (c) XRD patterns of the $CsPbBr_3$ PNCs/PVP@PS and $CsPbBr_3$ PNCs/PVP@PMMA powders. (d) FTIR spectrum of $CsPbBr_3$ PNCs/PVP@PMMA structures.

Flexible and superior hydrophobic polymers such as polystyrene (PS),[26−29] poly(vinylidene fluoride) (PVDF),[30−33] polydimethylsiloxane (PDMS),[34] and poly(methyl methacrylate) (PMMA)[35−37] could be used as encapsulation materials, which allow the PNCs to survive in *in vitro* and *in vivo* aqueous environments with high luminescence efficiency but no lead leakage. For example, in 2017, Zhang et al. reported a water-resistant microhemisphere strategy via embedding PNCs into the PS matrix for multicolor luminescence probes in live cells.[26] In 2018, Wang et al. designed a spray-assisted coil-globule transition method to encapsulate $CsPbBr_3$ PNCs into PMMA polymer nanospheres for cell imaging.[7] In 2020, Liu et al. designed core−shell PNCs/polymer nanospheres through an inverse emulsion method for advanced data encryption application.[35] In 2022, Wu et al. used poly (lactic-*co*-glycolic acid) (PLGA)-encapsulated PNCs as biological probes for rapid imaging of glioma cells.[38] Despite the efforts of scientists, it is still very challenging to realize highly stable, waterproof, small-sized nanoparticles with a high luminescence efficiency. Thus, there is an urgent need to propose a strategy to achieve encapsulated PNCs with high water resistance, high fluorescence efficiency, low lead leakage, and high biocompatibility.

In this work, we report an encapsulation strategy to fabricate $CsPbX_3$ (X = Cl, Br, and I) PNCs/PVP@PMMA structures by embedding $CsPbX_3$ PNCs into PMMA matrices. The synthesized $CsPbX_3$ PNCs/PVP@PMMA structures exhibit high stability and excellent fluorescence properties due to the controllable modulation of n-hexane. Additionally, the obtained $CsPbBr_3$ PNCs/PVP@PMMA structures emit green emissions with a PLQY of 70.24%, while the $CsPbBr_{0.6}I_{2.4}$ PNCs/PVP@PMMA phosphors show an optimal PLQY of 98.26%, which demonstrates an excellent potential for biophotoelectric applications. Moreover, the synthesized $CsPbX_3$ PNCs/PVP@PMMA structures show exceptional performance in cell imaging and white-light LED devices with red-green-blue emissions, water resistance, and free lead leakage. All these results may provide an excellent platform for fabricating future solid-state white light sources and full-color displays.

RESULTS AND DISCUSSION

Figure 1 illustrates the strategy for synthesizing the core-interfacial layer-shell structure of $CsPbX_3$ PNCs/PVP@PMMA particles with biocompatible and waterproof shells, which can be used for both bioimaging and LED applications. The *N*,*N*-dimethylformamide (DMF) precursor solution of CsBr and $PbBr_2$ was injected into a dichloromethane (DCM, low polarity) solution containing polyvinyl pyrrolidone (PVP) to form PVP-coated $CsPbBr_3$ PNCs at room temperature under vigorous stirring. PVP acts as the capping ligands to be physically absorbed on the surface of PNCs to form a protective layer, which not only enables PNCs to stabilize in DCM solution and controls the particle size of PNCs but also

https://doi.org/10.1021/acsami.4c06854
ACS Appl. Mater. Interfaces 2024, 16, 34167−34180

acts as an interfacial layer to be compatible with outer-PMMA polymers. The washed PVP-coated $CsPbX_3$ PNCs were then redispersed in a mixed solution of PMMA and DCM. Then, $CsPbBr_3$ PNCs/PVP@PMMA precipitates were formed by adding antisolvent n-hexane into the mixed solution at an optimal feeding ratio of 6:1 (Figure S1). After that, they were dried overnight at room temperature and then ground with a mortar and pestle to obtain the composite powders.

To demonstrate the formation process of the water-resistance and biocompatible core-interfacial layer-shell PNCs/PVP@PMMA structures, transmission electron microscopy (TEM) is used to characterize their microstructures at each stage. The TEM images and the inset size distribution are shown in Figure 2a, which exhibit that the $CsPbBr_3$ PNCs have been synthesized before the addition of the n-hexane solvent, and they possess a regular cubic morphology with an average edge length of 56.8 nm. In Figure 2b, the high-resolution TEM (HR-TEM) image demonstrates well-defined lattice fringes with the interplanar spacing of 0.58 nm, assigned to be the *d*-spacing of the (001) crystalline plane of cubic phase perovskite $CsPbBr_3$. A distinct thin shell can be observed in the enlarged $CsPbBr_3$ nanocubes, which is speculated to be due to the adsorption of PVP/PMMA colloidal polymers on the surface of PNCs, thereby facilitating the stable dispersion of $CsPbBr_3$ PNCs/PVP@PMMA without aggregation in weakly polar DCM. The TEM images of $CsPbX_3$ PNCs/PVP@PMMA composite powders were obtained by drop-casting the dilute ethanol solution onto ultrathin carbon-coated copper grids and drying them under an ambient atmosphere. The TEM images of $CsPbBr_3$ PNCs/PVP@PMMA in Figure 2c demonstrate that cubic $CsPbBr_3$ PNCs are uniformly embedded in the robust polymers, protecting them against outside ethanol invasion and electron beam irradiation. The interplanar spacing of a selected nanocube in a polymeric matrix is 0.42 nm, corresponding to the (110) crystalline plane of cubic phase $CsPbBr_3$. Figure S2 (Supporting Information) shows the HR-TEM images of $CsPbCl_{1.2}Br_{1.8}$ and $CsPbBr_{0.6}I_{2.4}$ PNCs/PVP@PMMA powders in ethanol, illustrating that the PNCs are fully encapsulated with the polymers. As depicted, the PNCs have lattice fringes with spacing distances of 0.398 and 0.419 nm for $CsPbCl_{1.2}Br_{1.8}$ and $CsPbBr_{0.6}I_{2.4}$ PNCs/PVP@PMMA, respectively. The surface topography of $CsPbBr_3$ PNCs/PVP@PMMA composites was also investigated by SEM (Figure 2e,f), from which it can be seen that the dispersed grains have approximately uniform sizes. Additionally, the energy-dispersive X-ray spectroscopy (EDS) mapping of $CsPbBr_3$ PNCs/PVP@PMMA is collected to identify the core−shell structure, as shown in Figure 2f_1−f_6. The C, N, and O elemental distributions show precise grain boundary profiles, mainly from the polymer shell layer formed by cross-linking interactions. The signals of Cs, Pb, and Br elements associated with the $CsPbBr_3$ PNCs have blurred boundaries and mainly originate from the inner-core regions of the grains, indicating that the polymer shell can completely encapsulate the PNCs.

The optical properties of the colloidal $CsPbX_3$ PNCs/PVP@PMMA (X = Cl, Br, I, or their mixture) can be tuned over the entire visible spectral range by varying the halide compositions. As shown in Figure 3a and Figure S3 (see Supporting Information), the PL emission and absorption spectra with different halogen ratios are plotted, respectively. It can be seen that the PL emission peaks can be continuously tuned from 429 to 677 nm, with the narrow fwhm changing from 16 to 27 nm, accordingly. These narrow emission peaks reveal an excellent homogeneity of size distribution and monochromaticity of colloidal $CsPbX_3$ PNCs/PVP@PMMA nanocrystals. The absorption spectra exhibit a regular blue or red shift, depending on the variation of the halogen compositions. Figure 3b presents the optical photographs of colloidal $CsPbX_3$ PNCs/PVP@PMMA and corresponding $CsPbX_3$ PNCs/PVP@PMMA powders with different halogen-dependent compositions under room light (upper) and 365 nm UV light (bottom), respectively. Therefore, the synthesized multicolor polymer-encapsulated PNCs hold great potential for optoelectronic applications, such as multicolor bioimaging, cell tracing, high-resolution displays, and indoor illumination. The measured absolute PLQY in DCM solution is only about 13.38% before $CsPbBr_3$ PNCs/PVP@PMMA solid precipitates formed. Thus, the relatively low light output could be ascribed to the reabsorption and multiple scattering effects caused by the assembled suspension of the cross-linked polymers and PNCs. Interestingly, the enhanced PLQY was acquired when the milled $CsPbX_3$ PNCs/PVP@PMMA powders were dispersed in a toluene solvent. In particular, the $CsPbBr_3$ PNCs/PVP@PMMA powders in toluene emit green emissions with an improved PLQY of 70.24%, while the red-emitting[39] $CsPbBr_{0.6}I_{2.4}$ PNCs/PVP@PMMA phosphors have a strikingly optimal PLQY as high as 98.26%. This observation is attributed to the effective defect passivation of the PVP interfacial layer and the protective effect of the outer shell layer on isolating the internal PNCs from the environment.

To further demonstrate the crystalline structure of the $CsPbBr_3$ PNCs/PVP@PMMA composites, the X-ray diffraction (XRD) patterns were acquired as shown in Figure 3c. The XRD patterns of $CsPbBr_3$ PNCs/PVP@PS as a control experimental group were also examined to understand the encapsulation effect of the polymer materials. It can be seen that all diffraction peaks coincide well with the standard PDF#54−0752 card of cubic phase $CsPbBr_3$. Both $CsPbBr_3$ PNCs/PVP@PS and PNCs/PVP@PMMA composites exhibit strong characteristic diffraction peaks at 15.1°, 21.4°, and 30.6°, corresponding to the (100), (110), and (200) planes of $CsPbBr_3$ perovskite nanocrystals, respectively. All of these results indicate that $CsPbBr_3$ perovskite nanocrystals always maintained the cubic phase even after the two-step encapsulation process. Also, a broad diffraction band ranging from 15° to 23° in the XRD pattern of the $CsPbBr_3$ PNCs/PVP@PS is associated with the presence of excess polymers.

The Fourier transform infrared spectroscopy (FTIR) was used to confirm the presence of PVP, which adsorbed to the PNCs and cross-linked with the PMMA outer polymer layer, producing a passivation effect on the surface defects and improving the crystalline quality of the PNCs (Figure 3d). The absorption peaks at 2943 and 2852 cm^{-1} could be ascribed to the stretching vibration of $-CH_3$ and $-CH_2$, while the peaks at 991, 754, 619, and 1454 cm^{-1} could be assigned to the C−H bending vibration. The strong 1730 cm^{-1} can be identified as the C═O carbonyl stretching vibration of the five-membered cyclic lactam structure of PVP.[40] Moreover, the band at 1645 cm^{-1} is associated with the C═O stretching vibration. Finally, the absorption band at 1253 cm^{-1} is related to the C−N bending vibration from the pyrrolidone structure of PVP.[41,42] The bands at 1149 cm^{-1} are ascribed to the C−O stretching vibration of the PMMA.[43] These results indicate the presence of the cross-linked polymers of PVP and PMMA on the surface of $CsPbBr_3$ PNCs.

https://doi.org/10.1021/acsami.4c06854
ACS Appl. Mater. Interfaces 2024, 16, 34167−34180

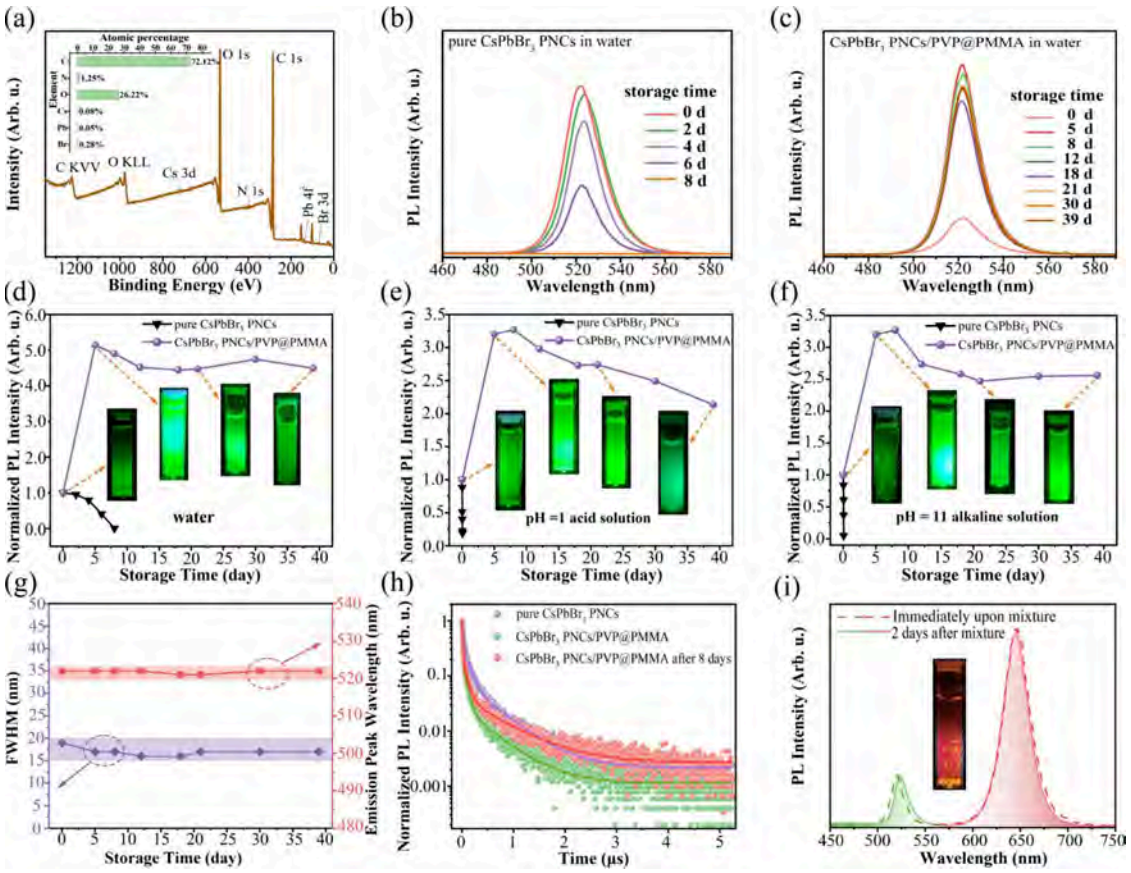

Figure 4. Stability performance of pure $CsPbBr_3$ PNCs and $CsPbBr_3$ PNCs/PVP@PMMA structures. (a) Full scan of the XPS spectrum. The insets show the atomic percentages of diversified elements. (b) Storage time-dependent PL spectra of pure $CsPbBr_3$ PNCs and (c) $CsPbBr_3$ PNCs/PVP@PMMA in deionized water. (d) Normalized PL intensity of pure $CsPbBr_3$ PNCs (black triangle) and $CsPbBr_3$ PNCs/PVP@PMMA (purple sphere) in deionized water, (e) acid solution (pH = 1), and (f) alkali solution (pH = 11) as a function of storage time, respectively. Insets are PL photographs of the $CsPbBr_3$ PNCs/PVP@PMMA solutions at different storage times within 39 days under a 365 nm UV-light excitation. (g) fwhm and PL emission peak wavelength of $CsPbBr_3$ PNCs/PVP@PMMA. (h) Time-resolved PL spectra of the pure $CsPbBr_3$ PNCs and $CsPbBr_3$ PNCs/PVP@PMMA (as-prepared and after 8 days) in water, respectively. (i) PL spectra of $CsPbBr_3$ and $CsPbBr_{0.6}I_{2.4}$ PNCs/PVP@PMMA mixed solution under a 365 nm UV-light excitation: immediately upon mixture (dotted-line) and 2 days after mixture (solid-line profile filled with color). The inset illustrates that two mixed composites dispersed in water for 2 days.

To analyze the chemical compositions and states of the $CsPbBr_3$ PNCs/PVP@PMMA, X-ray photoelectron spectroscopy (XPS) spectra were also performed, as shown in Figure 4a and Figure S4 (see the Supporting Information). The presence of Cs, Pb, Br, C, N, and O signals is confirmed by the full scan of the XPS spectrum (Figure 4a). The C, N, and O elements mainly originate from the coated polymer material (PVP) and the introduced DMF during the synthesis process. The measured atomic percentages of Cs, Pb, and Br are 0.08%, 0.05% and 0.28%, respectively, with an atomic ratio of approximately 1:1:3 (inset in Figure 4a). Based on structural characterizations, such as HR-TEM images, EDS mappings, XRD patterns, FTIR spectra, and XPS analysis, it can be concluded that the $CsPbBr_3$ PNCs/PVP@PMMA composites have been successfully synthesized.

To improve the practical applicability of lead halide perovskite nanocrystals, the degradation of their fluorescence properties in polar solvents (water) and acid and alkali aqueous solutions, which usually exist in organic organisms, should be addressed as a critical issue. An assumption of encapsulating $CsPbX_3$ PNCs into biocompatible shells to form the $CsPbX_3$ PNCs/PVP@PMMA, the dissociation of $CsPbX_3$ into Cs^+ and $[PbX_6]^{4-}$ in water due to its ionic properties will be suppressed. To assess the fluorescence stability in different surroundings of PNCs, the PL spectra and photographs of PNCs are monitored at various time intervals by dispersing 6 mg of PNC powders into 5 mL of water, acid, and alkali aqueous solutions, respectively. In addition, the stability and luminescence properties of $CsPbX_3$ PNCs/PVP@PMMA are compared in this work, and pure $CsPbBr_3$ PNCs as a control group are also prepared. The PL intensity of pure $CsPbBr_3$ PNCs decreased rapidly and even showed serious quenching within 8 days upon meeting deionized water (Figure 4b). In contrast, the $CsPbBr_3$ PNCs/PVP@PMMA abruptly increased within 5 days and then stayed relatively stable with some fluctuations within 39 days (Figure 4c). For a clear and intuitive comparison, the normalized PL intensities of pure $CsPbBr_3$ PNCs and $CsPbBr_3$ PNCs/PVP@PMMA dispersed in solution (based on their respective initial stages) are plotted as a function of the storage time, as shown in Figure 4d. It is observed that the relative fluorescence intensity of pure $CsPbBr_3$ PNCs in water dropped to only ~0.25% of the initial value within 8 days. In contrast, the relative PL intensity of $CsPbBr_3$ PNCs/PVP@PMMA in water is greatly enhanced over the initial fluorescence intensity value. Afterward, the PL intensity decreased slightly but remained high, maintaining a

https://doi.org/10.1021/acsami.4c06854
ACS Appl. Mater. Interfaces 2024, 16, 34167−34180

Table 1. Decay Times of Pure $CsPbBr_3$ PNCs and $CsPbBr_3$ PNCs/PVP@PMMA in Water and also $CsPbBr_3$ PNCs/PVP@PMMA in Water after 8 days by Tri-exponential Decay Function

sample	I_1	τ_1(ns)	I_2	τ_2(ns)	I_3	τ_3(ns)	t_{ave}(μs)
$CsPbBr_3$ PNCs	0.80	11.98	0.19	70.63	0.03	543.22	0.25
$CsPbBr_3$ PNCs/PVP@PMMA	0.36	101.80	0.58	17.16	0.08	549.60	0.31
$CsPbBr_3$ PNCs/PVP@PMMA after 8 days	0.77	11.21	0.20	79.55	0.04	718.85	0.41

fluorescence intensity value of 4.5 times the initial fluorescence intensity value after 39 days. The insets in Figure 4d show the PL photographs of $CsPbBr_3$ PNCs/PVP@PMMA in water for different storage times. This result indicates that fluorescence brightness has the same variation tendency as PL intensity over time. It is pointed out that the significant enhancement of PL intensity of $CsPbBr_3$ PNCs/PVP@PMMA in water is attributed to the synergistic effect of the effective passivation of surface defects from the interfacial layer and the hydrophobic interaction from outer-shell polymers. In fact, $CsPbX_3$ PNCs/PVP@PMMA powders, including green $CsPbBr_3$, blue $CsPbCl_{1.2}Br_{1.8}$, and red $CsPbBr_{0.6}I_{2.4}$ PNCs/PVP@PMMA in water can still exhibit bright fluorescence under 365 nm UV-light excitation even after 18 months of storage in water (Figure S5, see the Supporting Information). The PLQY of $CsPbBr_3$ PNCs/PVP@PMMA remains at 70.17 and 38.59% after 30 days and 18 months of storage in water, respectively. The full width at half-maximum (fwhm) and emission peak of PL spectra of $CsPbBr_3$ PNCs/PVP@PMMA in Figure 4g exhibit almost unchanged during the 39 days. Figure 4e,f plots the normalized PL intensity of the pure $CsPbBr_3$ PNCs and $CsPbBr_3$ PNCs/PVP@PMMA as a function of the storage time in acid (pH 1) and alkali (pH 11) aqueous solutions, respectively. It is found that the PL intensity of the pure $CsPbBr_3$ PNCs is almost quenched when they are immersed in acid or alkali solutions for 1 h. Nevertheless, the fluorescence intensity of $CsPbBr_3$ PNCs/PVP@PMMA in acid or alkali solutions exhibits trends similar to that in deionized water. After 39 days of storage in acidic and alkaline solutions, the PL intensity increased to approximately 2.1 and 2.5 times the initial values, respectively. Figure 4e,f insets display the digital photographs of $CsPbBr_3$ PNCs/PVP@PMMA immersed in acid or alkaline solutions for different monitoring periods. After 39 days, they can still emit bright green fluorescence visible to the naked eye under UV light, effectively proving enhanced resistance to harsh acid and alkali environments. It is suggested that the polymer shells can effectively prevent the aggregation of PNCs and block erosion from the external environment.

The time-resolved PL spectra of the pure $CsPbBr_3$ PNCs and $CsPbBr_3$ PNCs/PVP@PMMA are obtained, as shown in Figure 4h. The decay curves of the time-resolved PL spectra could be well-fitted by a triple-exponential decay function, as follows:

$$I = A_1\exp\left(-\frac{t}{\tau_1}\right) + A_2\exp\left(-\frac{t}{\tau_2}\right) + A_3\exp\left(-\frac{t}{\tau_3}\right) \quad (1)$$

where τ_1 is the fast component and τ_2 and τ_3 the middle and slow components, respectively. Additionally, A_1, A_2, and A_3 are the corresponding amplitudes, representing the respective proportions of each component (Table 1). It indicates that there are two main routes in the recombination process: the fast component τ_1 is mainly attributed to the radiative recombination of photons from the conduction band to the valence band. While the middle and slow components τ_2 and τ_3 are ascribed to the nonradiative recombination of photons from the conduction band to shallow-level surface defects as well as from defects to defects, respectively.[44,45] The average lifetimes (τ_{ave}) could be derived from the following formula:

$$\tau_{ave} = \frac{A_1\tau_1^2 + A_2\tau_2^2 + A_3\tau_3^3}{A_1\tau_1 + A_2\tau_2 + A_3\tau_3} \quad (2)$$

The fitted results indicate that the $CsPbBr_3$ PNCs/PVP@PMMA in aqueous solution has an average PL lifetime of about 0.31 μs, which is longer than that of 0.25 μs for the pure $CsPbBr_3$ PNCs. In addition, the lifetime of $CsPbBr_3$ PNCs/PVP@PMMA in water was also detected after 8 days as shown in Figure 4h, which shows a longer average lifetime of 0.41 μs than that of $CsPbBr_3$ PNCs/PVP@PMMA initially in aqueous solution. Defects are related to nonradiative recombination, which brings about faster relaxation. The longer average lifetime of $CsPbBr_3$ PNCs/PVP@PMMA compared to pure $CsPbBr_3$ PNCs suggests that the defect density is effectively reduced due to the coexistence of the interfacial and the outer shell layer. Thus, the photogenerated excitons are more inclined to radiative recombination. Additionally, the prolonged lifetimes of $CsPbBr_3$ PNCs/PVP@PMMA after 8 days in water as compared to the initial stage also manifests that the nonradiative recombination is suppressed, which is consistent with the enhancement of the fluorescence intensity with a period of storage time. It is worth noting that the $CsPbBr_3$ PNCs/PVP@PMMA has an extremely long average PL lifetime in the order of microseconds, which is associated with the large sizes of the PNCs in aqueous solution.[44] Figure 4i shows the PL spectra of the green $CsPbBr_3$ PNCs/PVP@PMMA and red $CsPbBr_{0.6}I_{2.4}$ PNCs/PVP@PMMA mixed solutions under a 365 nm laser excitation. The dashed line represents the spectrum of the immediately mixed solution, where the emission peaks at 520 and 645 nm arise from $CsPbBr_3$ PNCs/PVP@PMMA and $CsPbBr_{0.6}I_{2.4}$ PNCs/PVP@PMMA, respectively. The solid line represents the PL emission spectrum after 2 days. They show similar spectral shapes to the immediately mixed solution but with a negligible shift in the peaks due to the relatively long storage time. This result indicates that the encapsulation effect restrains the halogen anion exchange reaction. The insets of Figure 4i show the photograph of the mixed $CsPbBr_3$ PNCs/PVP@PMMA with $CsPbBr_{0.6}I_{2.4}$ PNCs/PVP@PMMA powders in water after 2 days.

Thus, the chemical stability of $CsPbX_3$ PNCs/PVP@PMMA powders in polar solvents and acid/ alkaline solutions is greatly improved, and the halide-anion exchange reaction is suppressed. The protective layer formed by the cross-linking interaction of the long chains PVP and PMMA has typical hydrophobic properties, which can efficiently isolate the internal vulnerable PNCs from external water molecules and various water-soluble ions. The performance degradation of

https://doi.org/10.1021/acsami.4c06854
ACS Appl. Mater. Interfaces 2024, 16, 34167−34180

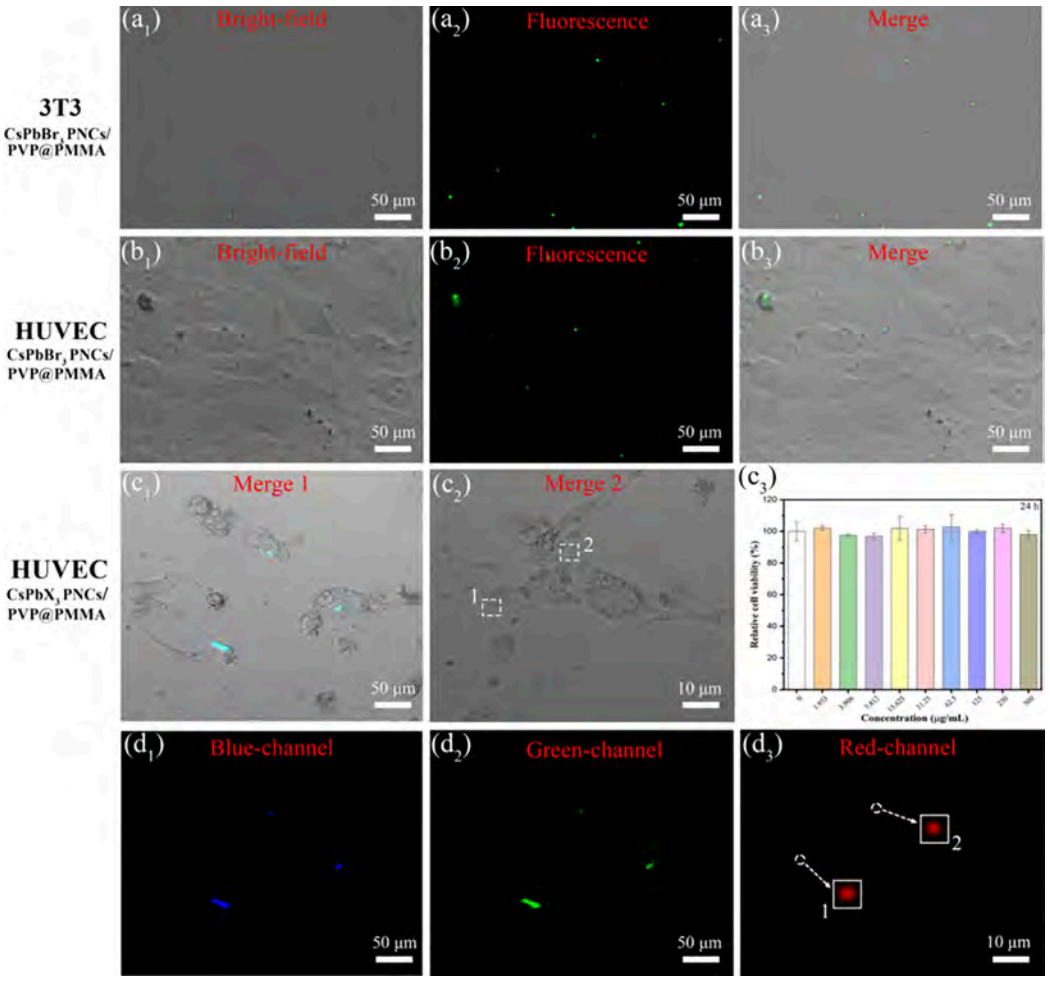

Figure 5. Confocal fluorescence imaging by 3T3 cells and HUVEC cells. (a_1–a_3) Confocal fluorescence images of 3T3 cells and (b_1–b_3) HUVEC cells incubated with $CsPbBr_3$ PNCs/PVP@PMMA after 24 h, respectively. (a_1, b_1) Bright-field images, (a_2, b_2) fluorescence images, and (a_3, b_3) merged images. (c_1, c_2) Merged images in different endocellular regions and (c_3) cytotoxicity. The blended $CsPbX_3$ PNCs/PVP@PMMA powders are used to treat the human HUVEC cells after 24 h. (d_1–d_3) Corresponding individual fluorescence images in the human HUVEC cells.

$CsPbX_3$ PNCs is inhibited due to the robustness of the protective layer.

Additionally, lead leakage into water during the dissociation process of $CsPbX_3$ PNCs will cause severe damage to the environment and even living organisms, severely limiting their utilization. Inductively coupled plasma optical emission spectroscopy (ICP-OES) is also conducted to evaluate the lead contents after dispersing $CsPbBr_3$ PNCs/PVP@PMMA in deionized water. The release of Pb elemental amount is 0.024 ppm (mg L^{-1}) after 2 h and only up to 0.061 ppm (mg L^{-1}) after 100 days of storage in water. The trace lead leakage in water confirms the validity of the encapsulation and provides safety assurance for *in vitro* and *in vivo* labeling and bioimaging.

Considering the low lead-leakage and low photobleaching properties of $CsPbX_3$ PNCs/PVP@PMMA, which can achieve long-term fluorescence in harsh environments, it is highly likely to be used as a luminescence probe for multicolor bioimaging. To further validate its feasibility, 3T3 and HUVEC cells are chosen to treat $CsPbBr_3$ PNCs/PVP@PMMA powders at concentrations ranging from 0 to 500 μg mL^{-1} in cell culture fluid for *in vitro* cytotoxicity assay and live cell imaging. Since the average particle size of $CsPbBr_3$ PNCs/PVP@PMMA is about 56.8 nm, $CsPbBr_3$ PNCs/PVP@PMMA may be taken up by cells through endocytosis. As shown in Figure 5a,b, the confocal fluorescence images illustrate the phagocytosis of nanocrystals at a concentration of 31.25 μg mL^{-1} by 3T3 cells and HUVEC cells after 24 h, respectively. These merged images show strong green fluorescence spots in the cytoplasm under 405 nm excitation, indicating the successful entry of $CsPbBr_3$ PNCs/PVP@PMMA into living cells. Throughout the incubation process, the cells ingested with the nanocrystals remained spindle-shaped without significant damage, and the intracellular fluorescence intensities did not exhibit apparent attenuation. Further, multicolor cell imaging was also performed by culturing HUVEC cells with blended $CsPbX_3$ PNCs/PVP@PMMA powders ($CsPbCl_{1.2}Br_{1.8}$, $CsPbBr_3$, and $CsPbBr_{0.6}I_{2.4}$ PNCs/PVP@PMMA powders with the mass ratio of 1:1:1). According to the merged images in Figure 5c_1,c_2, the blue, green, and red fluorescence in different intracellular regions can be observed after the cell incubation of 24 h, indicating that the cells can be successfully labeled and tracked by multicolor phosphors. The corresponding individual fluorescence images are also shown in Figure 5d_1–d_3. Subsequently, the cytotoxicity of the 3T3 cells and HUVEC cells treated with $CsPbBr_3$ PNCs/PVP@PMMA and blended $CsPbX_3$ PNCs/PVP@PMMA powders was evaluated with CCK-8 assay for 24 h, respectively (Figure 5c_3 and Figure S6, see the Supporting Information). The cytotoxicity test results

https://doi.org/10.1021/acsami.4c06854
ACS Appl. Mater. Interfaces 2024, 16, 34167−34180

Table 2. Comparison of Various Properties of Different Core−Shell Structures

structures	method	PLQY	stability (PL intensity)	stability (PLQY)	lead-leakage in water	cytotoxicity(viability)	WLED	NTSC	CRI	efficiency (Lm W^{-1})	ref
$CsPbX_3$ PNCs/PVP@PMMA (X = Cl,Br, and I)	two-step encapsulation process	98.26%	4.5, 2.1 and 2.5 times of the initial value after 39 days in water, acid (pH = 1) and alkali (pH = 11) aqueous solutions, respectively	70.71% after 30 days in water; 38.5% 18 months in water	0.024 ppm(mg L^{-1}) after 2 h; 0.061 ppm (mg L^{-1}) after 100 days	>96% (0−500 μg mL^{-1})	$CsPbBr_3$ PNCs/PVP@PMMA+ $CsPbBr_xI_{1-x}$PNCs/PVP@PMMA and blue-emitting LED chip	115%	83.7	3.45	this work
PLGA-$CsPbBr_3$	ligand-assisted reprecipitation technique	87%	98% after 30 days	80.38% after 30 days in water	——	——	——	——	——	——	38
CPB@PMMA	spray-assisted coil-globule transition method	73%	81% after 80 days	——	——	99−92% (20−60 μg mL^{-1})	——	——	——	——	7
$CsPbX_3$@DOPC (phospholipid micelles) (X = Cl, Br, and I)	film hydration method	——	49.79% after 7 days in water; in the 95th hour retains 59.27% of that in the 48th hour in acid (pH = 5);alkaline solution keeps 32.97% of the initial intensity after 34 h	——	——	>94% (1670 nmol mL^{-1})	——	——	—	——	6
CPB−SiO_2@SiO_2 NPs	ligand-assisted reprecipitation	——	92% after 14th day	——	0.0002 ppm (mg L^{-1}) after 14 days	>90% (0−100 μg mL^{-1})	——	——	——	——	52
$CsPbBr_3$/mPEG-NH_2	ligand-assisted reprecipitation technique	41%	1.6 times of the initial value after one day	Increased to 41% a week later	——	95% (80 μg mL^{-1})	——	——	——	——	44
$CsPbBr_3$@SiO_2	the wet chemical method	10.2%	~80% after 24 h	——	——	~95% (25 μg mL^{-1})	——	——	——	——	46
$CsPbBr_3$@PEG-PCL	dispersion precipitation−dispersion method	42.7%	85−88% after 15 days,even under acidic (pH = 5.0) and basic (pH = 8.0) conditions	The PLQY only decreased from 54.1% to 48.0% after 20 days	——	>90% (300 μg mL^{-1})	——	——	——	——	47
$CsPbBr_3$/$CsPb_2Br_5$	simple water-assisted chemical transformation	80%	45% after 110 h	——	76.9 ppm (mg L^{-1}) after 24 h	89% (100 μg mL^{-1})	——	——	——	——	49
CPB@PMMA	facile solvent evaporation encapsulation	——	91% after 30 days	——	0.0041 ppm (mg L^{-1}) for 12 h	98.3% (100 μg mL^{-1})	——	——	——	——	50
PVP-PQD@SiO_2@C_{18}-PC	a simple and highly successful coating strategy	41.6%	~98% after 10 days	——	——	>89% (0−100 μg mL^{-1})	——	——	——	——	5
$CsPbBr_3$/$CsPb_2Br_5$@SiO_2−Brij58	encapsulation in water	68.05%	1.1 times of the initial value after 60 days	——	——	94.2% (32 μg mL^{-1})	——	——	——	——	53
$CsPbX_3$ PNCs/PVP@PS (X = Cl, Br, and I)	room-temperature solution self-assembly approach	27%	stay almost the same using 374 nm laser for 10 h	——	——	~100% (0−35 μg mL^{-1})	——	——	——	——	26
$CsPbBr_3$: Cs_4PbBr_6@CS	water-triggered method	——	increased 41% on 35th day	——	——	>90% (0−20 μg mL^{-1})	——	——	——	——	51
$CsPbX_3$-PQDs/MPMs@SiO_2 (X = Cl, Br, and I)	the hydrolysis-encapsulation strategy	84%	~48% after 30 days in water; still emit distinctly fluorescence in acid (pH = 1) and alkaline (pH = 11) solution more than 10 days	80% after 120 h	——	——	$CsPbBr_3$-PQDs/MPMs@SiO_2 + red (Sr,Ca)$AlSiN_3$:Eu	>100%	——	81	62

ACS Appl. Mater. Interfaces 2024, 16, 34167−34180 https://doi.org/10.1021/acsami.4c06854

Table 2. continued

structures	method	PLQY	stability (PL intensity)	stability (PLQY)	lead-leakage in water	cytotoxicity(viability)	WLED	NTSC	CRI	efficiency (Lm W^{1-})	ref
							phosphors + blue GaN chip				
$CsPbBr_3$@$CsPb_2Br_5$	in situ ice-confined freeze−thaw strategy	95%	80% for 7 days at 4 °C	——	——	——	$CsPbBr_3$@$CsPb_2Br_5$ mixed with PMMA on UV-LEDs chip as green-emitting LED	——	——	——	63
$MAPbBr_3$@SiO_2/PVDF	double-shell encapsulation strategy	85.5%	83% of the original intensity after 20 min and 55% after 2 h	——	——	——	green $MAPbBr_3$@SiO_2/PVDF NPs + red KSF + blue GaN chip	120%	——	147.5	30
$CsPbBr_3$@SiO_2	one-pot hot-injection strategy	87%	~90% after 30 days	——	——	——	green $CsPbBr_3$@SiO_2 + red $CsPbBr0.6I_{2.4}$@SiO_2 NCs + blue GaN chip	——	~90	~55	64
$CsPbBr_3$−PSZ	simple one-step in situ synthesis and encapsulation method	84.7%	95% of the initial intensity during 72 h at 100 °C	——	——	——	$CsPbBr_3$−PSZ + ideal red emitter + blue emitter	133%	——	——	65
$CsPbX_3$@pyrophyllite (X = Cl, Br, and I)	postassembly synthesis method	78%	92% after 6 days; 97% more than 5 months;	——	0.09 ppm (mg L^{-1}) after 30 days	——	$CsPbBr_3$@pyrophyllite + $CsPbBrI_2$@pyrophyllite + InGaN blue chip	117%	80.7	84	66
$CsPbBr_3$@SiO_2	one-step in situ method under room temperature	~75%	53% after 60 min under heating of 80 °C; 87% after 30 min in ethanol.	——	——	——	$CsPbBr_3$@SiO_2 QDs + AgInZnS QDs + InGaN blue chip	——	91	40.6	67
$CsPbBr_3$@ZrO_2 NCs	modified supersaturated recrystallization method	80%	81% after 90 min under heating of 60 °C;70% after 70 min in water	——	——	——	$CsPbBr_3$@ZrO_2 NCs + $CaAlSiN_3$:Eu^{2+} + InGaN blue chip	——	——	64	68
$CsPbBr_3$- DA QDs	modified hot-injection method	96%	66% after 90 min in ethanol;	75.2% after 7 days in water	——	——	$CsPbBr_3$- DA QDs + AgInZnS QDs + InGaN blue chip	——	93	64.8	69
$CsPbBr_3$@Cs_4PbBr_6/SiO_2 NCs	room temperature sol−gel method	92%	79% for 60 min in ethanol; 77% after 120 min in water	——	——	——	$CsPbBr_3$@Cs_4PbBr_6/SiO_2 NCs + AgInZnS QDs + InGaN blue chip	——	91	59.87	70

https://doi.org/10.1021/acsami.4c06854
ACS Appl. Mater. Interfaces 2024, 16, 34167−34180

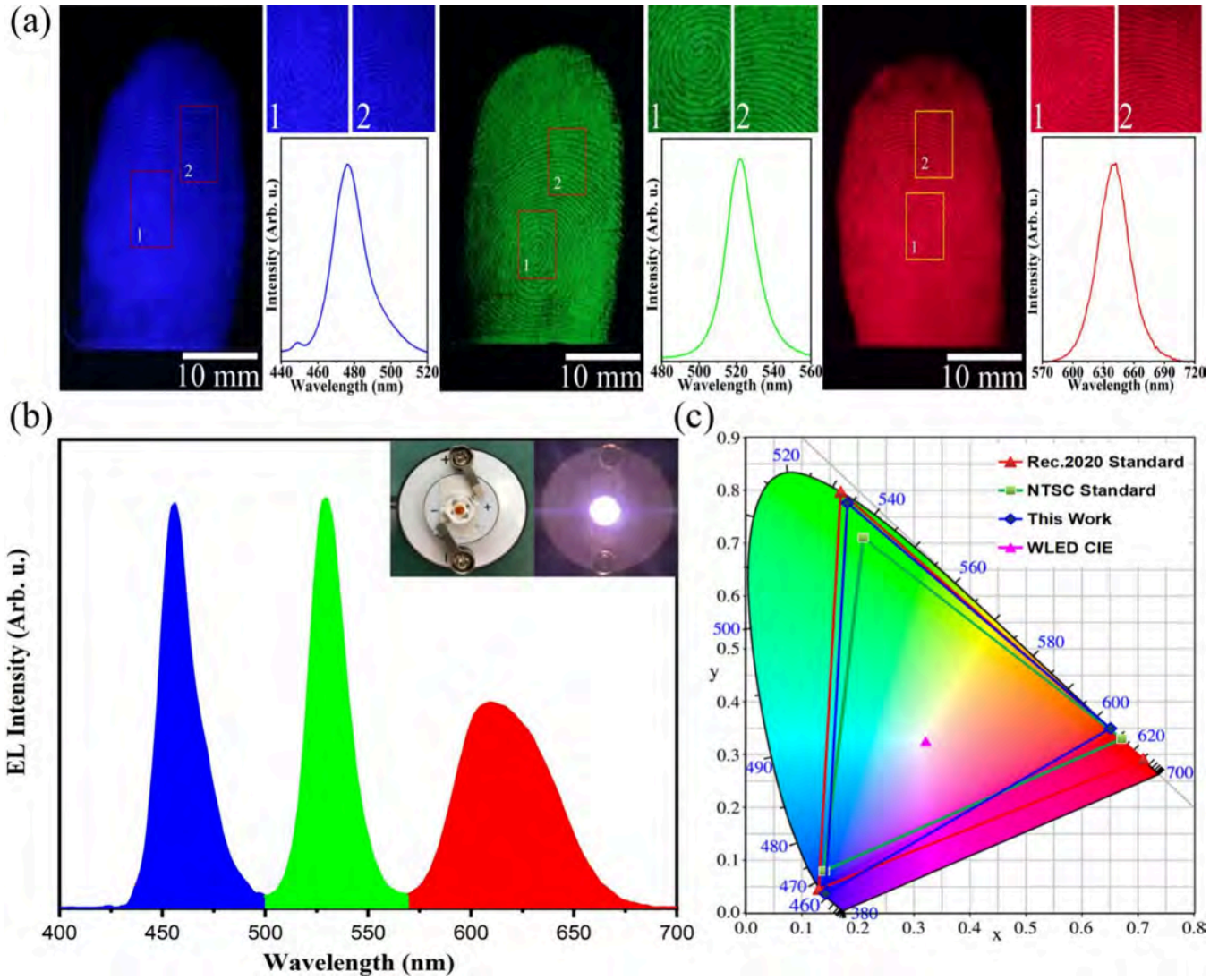

Figure 6. White light-emitting performance of the $CsPbX_3$ PNCs/PVP@PMMA structures. (a) Latent fingerprint images of tunable composition $CsPbX_3$ (X = Cl, Br, and I) PNCs/PVP@PMMA powders under 365 nm UV-light illumination. (b) EL spectra of $CsPbX_3$ PNCs/PVP@PMMA-based WLED at 20 mA. (c) 1931 CIE chromaticity diagram.

show that the viability of human HUVEC cells treated with $CsPbBr_3$ PNCs/PVP@PMMA and blended $CsPbX_3$ PNCs/PVP@PMMA powders could exceed 96.3% and 96.8%, respectively, when exposed to the PNC concentration ranging from 0 to 500 μg mL^{-1}. In addition, 94.4% of 3T3 cells are survivable within 24 h after exposure to the $CsPbBr_3$ PNCs/PVP@PMMA PNC at concentrations of 0−250 μg mL^{-1}, but at concentrations up to 500 μg mL^{-1}, the survival rate is 64%. Here, we compare the various properties of core−shell structures, as shown in Table 2, indicating that the $CsPbX_3$ PNCs/PVP@PMMA structures have low cytotoxicity and long-term emission. It is worth mentioning that our cytotoxicity assessment is relatively broad compared to other reports, i.e., the cell viabilities were tested at PNC concentrations much higher than 100 μg mL^{-1}.[46−48] These results indicate that $CsPbX_3$ PNCs/PVP@PMMA structures are suitable for general cellular labeling, tracking, and probing and can ensure almost no toxic lead-leakage during prolonged live cell incubation.[49−53]

In addition, latent fingerprint recognition is conducted by using representative multicolor $CsPbX_3$ PNCs/PVP@PMMA due to its enhanced luminescence properties and low cytotoxicity. As shown in Figure 6a, a well-resolved multicolor pattern configuration between the ridge and furrow is exhibited. The distinguishable latent fingerprint image contrast is mainly attributed to the electrostatic adsorption between $CsPbX_3$ PNCs/PVP@PMMA composites and surface oil secretion of fingerprints in the ridges as well as the electrostatic repulsion in the furrows caused by hydrophobic effects of the PNCs surface polymers.[54,55]

In order to further demonstrate the potential multifunctional applications of $CsPbX_3$ PNCs/PVP@PMMA in optoelectronics devices, a prototype phosphor-converted WLED was successfully prepared by encapsulating the composites of $CsPbBr_3$ PNCs/PVP@PMMA and $CsPbBr_{0.6}I_{2.4}$ PNCs/PVP@PMMA phosphors onto a blue-emitting InGaN LED chips with UV-cured adhesives. Although there are many reports on the fabrication of WLEDs[56,57] based on PNCs, many researchers rely on combining green-emitting $CsPbBr_3$ with commercial red-emitting phosphors (such as $K_2SiF_6:Mn^{4+}$ and $(Sr, Ca)AlSiN_3:Eu^{2+}$).[58] The aforementioned halogen anion exchange reaction is proven to be effectively inhibited by using

https://doi.org/10.1021/acsami.4c06854
ACS Appl. Mater. Interfaces 2024, 16, 34167−34180

the $CsPbX_3$ PNCs/PVP@PMMA composites with the core-interfacial layer-shell structures.[59] The electroluminescence (EL) spectrum is shown in Figure 6b, which consists of three distinct emission bands, with a narrow emission peak at 456 nm arising from the blue LED chip, a green emission peak at 530 nm originating from the $CsPbBr_3$ PNCs/PVP@PMMA phosphors, and a relatively board red emission peak at 610 nm ascribing to the $CsPbBr_{0.6}I_{2.4}$ PNCs/PVP@PMMA fluorescent powders. The thermal stability of the iodine-based perovskite phosphor with the $CsPbBr_{0.6}I_{2.4}$ PNCs/PVP@PMMA structure is relatively poor, resulting in degradation of the luminescence performance of the LED at higher driving currents. It is speculated that the fluorescence degradation may be caused by the rising temperature around the PNCs since the increase of the injection current leads to an elevation of the junction temperature.[60] Here, the WLED device is measured at an operating voltage of 2.5 V and a current of 20 mA. The device acquired a relatively low luminous efficiency of 3.54 lm/W compared to previous publications but is acceptable for perovskite PNCs-based LED devices.[61−66] By optimally adjusting the ratio of PNCs between green and red phosphors, warm-white light emission could be generated with a correlated color temperature (CCT) of 6061 K, a Commission Internationale de L'Eclairage (CIE) color coordinate of (0.321, 0.325), and a color rendering index (CRI) of 71.3, as shown in Figure 6c. Additionally, we chose another red phosphor $CsPbBr_{0.7}I_{2.3}$ PNCs/PVP@PMMA with a different halogen composition to be mixed with green phosphor $CsPbBr_3$ PNCs/PVP@PMMA to prepare the LED devices, which exhibits a relatively high CRI of 83.7, as shown in Figure S7. To further increase the thermal stability of WLEDs, we proposed that the WLEDs could be fabricated by mixing green $CsPbBr_3$ PNCs/PVP@PMMA phosphors with commercial red powder ($K_2SiF_6:Mn^{4+}$). Figure S8a,b presents the EL spectra of the fabricated WLEDs and also plots the EL intensity as a function of different driving currents (from 20 to 120mA), indicating that the EL intensity gradually increases with the increase of the driving current. The results confirm that the $CsPbX_3$ PNCs/PVP@PMMA are suitable as a color converter of the WLED. The anion exchange and concentration quenching effects could be solved by using the composites with the $CsPbX_3$ PNCs/PVP@PMMA core-interfacial layer-shell structure. Figure 6c also depicts the wide color gamut of the constructed WLED devices, which encompass 115% of the National Television Systems Committee (NTSC) standard in the CIE 1931 color space and 85.5% of the Ultra high-definition Television (UHDTV) in the CIE Rec.2020 color space, which may have great potentials in the fields of solid-state lighting and displays.[67−70]

CONCLUSIONS

In summary, we report a novel encapsulated strategy to realize $CsPbX_3$ PNCs/PVP@PMMA with a core-interfacial layer-shell structure. The obtained $CsPbX_3$ PNCs/PVP@PMMA structures exhibit high water resistance, high polar solvent stability, low lead-leakage, and good biocompatibility. The $CsPbX_3$ PNCs/PVP@PMMA structures exhibit high emission efficiency with excellent stability even after being in water for 18 months. Moreover, the $CsPbX_3$ PNCs/PVP@PMMA structures show cell imaging performance with long-term strong fluorescence and low toxicity in HUVEC and 3T3 cells, respectively. The WLED devices based on these $CsPbBr_3$ and $CsPbBr_{0.6}I_{2.4}$ PNCs/PVP@PMMA structures exhibit white-light emissions. In the next work, the thermal stability degradation and luminous efficiency of $CsPbX_3$ PNCs/PVP@PMMA-based WLED devices need to be further improved for practical applications in integrated optoelectronic and bioelectronics devices.

EXPERIMENTAL SECTION

Materials. CsX, PbX_2, PVP (Polyvinylpyrrolidone, MW 58000), PMMA (poly(methyl methacrylate)), and PS (polystyrene) were purchased from Aladdin and used as received without further purification. The DMF (*N*,*N*-dimethylformamide, AR grade) was purchased from Tianjin Fuyu Fine Chemical Co. Ltd. DCM (Dichloromethane, AR grade) was purchased from Tianjin Damao Chemical Reagent Factory.

Synthesis of $CsPbX_3$ PNCs/PVP@PMMA. As for the synthesis of $CsPbBr_3$ PNCs/PVP@PMMA, the 0.445 mmol CsBr and 0.445 mmol $PbBr_2$ were dissolved in 10 mL of DMF and stirred thoroughly at 25 °C until completely dissolved; then, 1 mL of the above solution was rapidly injected into 10 mL of DCM solution containing 0.25 g of PVP in a round-bottom flask under vigorous stirring. Subsequently, the solution was centrifuged at 7000 rpm for 5 min to collect the precipitates. Then, the precipitates were redispersed in 10 mL of DCM solution containing 0.1 g of PMMA and stirred for 2 h at 25 °C. Next, the clear yellow PNC colloids were obtained in DCM solution. The $CsPbX_3$ PNCs/PVP@PMMA were collected by adding the appropriate amount of n-hexane into colloidal PNCs (the volume ratio of colloidal PNCs to n-hexane is about 1:6) until the liquid supernatant turned clear. Finally, these $CsPbX_3$ PNCs/PVP@PMMA composites were dried in air by solvent evaporation and then ground into powders in a mortar. These powders were put into water to test their water resistance and used in applications such as live cell imaging, latent fingerprinting, and WLED devices.

Synthesis of $CsPbX_3$ PNCs. The pure $CsPbBr_3$ PNCs were also fabricated as a control group via a similar supersaturated recrystallization method. Briefly, the precursor solution was prepared by mixing 0.445 mmol of CsBr, 0.445 mmol of $PbBr_2$, 0.25 mL of OA, and 0.5 mL of OAm in 10 mL of DMF. Then, 8 mL of DMF precursor solution containing $PbBr_2$, CsBr, OA, and OAm was injected into 10 mL of DCM solvent without PVP and/or PMMA at room temperature with vigorous stirring. Subsequently, the solutions were centrifuged at 8000 rpm for 5 min to collect the precipitates. The precipitates were redispersed into water for the fluorescence properties and PL lifetimes.

Fabrication of WLEDs. $CsPbBr_3$ PNCs/PVP@PMMA green phosphor powders and $CsPbBr_{0.6}I_{2.4}$ (or $CsPbBr_{0.7}I_{2.3}$) red phosphor powders were mixed in the ratio of 2:1 with UV curing glue (the mass of total powders to glue is 1:1) and then stirred vigorously to form a homogeneous mixture. The mixture was dropped on an InGaN-based blue-emitting LED chip (3 W, 455−460 nm, San'an Optoelectronics Co., Ltd.) and dried at 150 °C for 1 h. So far, the WLEDs based on red and green phosphors on the blue LED chips have been fabricated for optoelectronic measurements.

Characterization Methods. The morphologies of nanoparticles were characterized using a transmission electron microscopy (TEM) JEOL JEM-F200 microscope at 200 kV accelerating voltage. Scanning electron microscopy (SEM) images were acquired by a ZEISS Sigma 300. The photoluminescence (PL) spectra, decay curves, and absolute photoluminescence quantum yield (PLQY) were obtained on an FLS5 fluorescence spectrophotometer with an excitation wavelength of 365 nm at room temperature. Fourier transform infrared (FTIR) spectra were tested on a Nicolet is5/is10 FT-IR spectrometer in the range of 4000−600 cm^{-1}. X-ray diffraction (XRD) patterns were performed by a Bruker D8 using Cu Ka radiation (λ= 0.154 nm) operating at 40 kV.

Cell Culture and Cell Imaging. HUVEC and 3T3 cells were cultured in Dulbecco's modified Eagle's medium (DMEM) supplemented with 10% FBS in a 5% CO_2 humidity incubator at 37 °C. HUVEC cells were seeded in 96-well plates at a density of 6×10^3 cells/well and cultured in 5% CO_2 at 37 °C for 24 h in a cell

https://doi.org/10.1021/acsami.4c06854
ACS Appl. Mater. Interfaces 2024, 16, 34167−34180

culture medium (i-Cell-h110−001b). After the medium was removed, cells were incubated with 1 mL of fresh medium and 10 μL of PBS containing $CsPbBr_3$ PNCs/PVP@PMMA (pH 7.4) for 24 h. Prior to imaging, the 3T3 and HUVEC cells were gently washed with PBS 3 times. Fluorescent images were recorded using a × 60 objective lens, and the images were processed using the Olympus FV10-ASW 1.6 viewer software.

Cell Toxicity. The standard Cell Counting Kit-8 (CCK-8) assay was employed to determine the relative cell viability. 3T3 and HUVEC cells were seeded in 96-well microplates at 6×10^3 cells/well in 150 μL of DMEM containing 10% FBS at 37 °C. After 24 h of incubation later, the culture medium was removed with 100 μL of fresh medium containing various concentrations of $CsPbBr_3$ PNCs/PVP@PMMA ranging from 0 to 500 mg mL^{-1}. Finally, the cell viability was examined by adding 80 μL to 96-well plates at an absorption wavelength of 450 nm.

■ ASSOCIATED CONTENT

Supporting Information

The Supporting Information is available free of charge at https://pubs.acs.org/doi/10.1021/acsami.4c06854.

Different feeding ratios of n-hexane to the mixed solution of colloidal PNCs; HRTEM images of $CsPbCl_{1.2}Br_{1.8}$ and $CsPbBr_{0.6}I_{2.4}$ PNCs/PVP@PMMA powders in ethanol; absorption spectra with different halogen ratios of $CsPbX_3$ PNCs/PVP@PMMA structures; XPS spectra of $CsPbBr_3$ PNCs/PVP@PMMA; fluorescence photographs of $CsPbX_3$ PNCs/PVP@PMMA powders in water as-prepared and after 18 months of storage; cytotoxicity test of HUVEC cells and 3T3 cells treated by $CsPbBr_3$ PNCs/PVP@PMMA; EL spectra of WLEDs based on $CsPbBr_3$ and $CsPbBr_{0.7}I_{2.3}$ PNCs/PVP@PMMA phosphors; EL spectra of WLEDs based on $CsPbBr_3$ PNCs/PVP@PMMA and red powder phosphors K_2SiF_6:Mn^{4+} the intensity variation of EL spectra under the different driving current from 20 to 120 mA (PDF)

■ AUTHOR INFORMATION

Corresponding Authors

Rui Zhang − *Department of Physics, Taiyuan University of Science and Technology, Taiyuan 030024, China;* orcid.org/0000-0002-2968-0682; Email: zrzx_0921@tyust.edu.cn

Pengfei Guo − *Department of Materials Science and Engineering and State Key Laboratory of Terahertz and Millimeter Waves, City University of Hong Kong, Hong Kong 999077, China; College of Electronic Information and Optical Engineering, Taiyuan University of Technology, Taiyuan 030024, China;* orcid.org/0000-0002-4785-0753; Email: guopengfei2010@126.com

Authors

Ao Yan − *Department of Physics, Taiyuan University of Science and Technology, Taiyuan 030024, China*

Haiyun Liu − *Department of Physics, Taiyuan University of Science and Technology, Taiyuan 030024, China*

Zehua Lv − *Department of Physics, Taiyuan University of Science and Technology, Taiyuan 030024, China*

Mengqing Hong − *The Institute of Technological Sciences, Wuhan University, Wuhan 430072, China*

Zhenxing Qin − *Department of Physics, Taiyuan University of Science and Technology, Taiyuan 030024, China*

Weijie Ren − *Department of Physics, Taiyuan University of Science and Technology, Taiyuan 030024, China*

Zhaoyi Jiang − *Department of Physics, Taiyuan University of Science and Technology, Taiyuan 030024, China*

Mingkai Li − *School of Materials Science and Engineering, Hubei University, Wuhan 430062, China;* orcid.org/0000-0002-4037-1784

Johnny C. Ho − *Department of Materials Science and Engineering and State Key Laboratory of Terahertz and Millimeter Waves, City University of Hong Kong, Hong Kong 999077, China;* orcid.org/0000-0003-3000-8794

Complete contact information is available at: https://pubs.acs.org/10.1021/acsami.4c06854

Notes

The authors declare no competing financial interest.

■ ACKNOWLEDGMENTS

This work was supported by the National Natural Science Foundation of China (NSFC, Grant Nos. 52373246 and 12105206) and the Fundamental Research Program of Shanxi Provinces (Nos. 20210302123221, 202103021224268, and 202303021222175).

■ REFERENCES

(1) Li, X.; Wu, Y.; Zhang, S.; Cai, B.; Gu, Y.; Song, J.; Zeng, H. $CsPbX_3$ Quantum Dots for Lighting and Displays: Room-Temperature Synthesis, Photoluminescence Superiorities, Underlying Origins and White Light-Emitting Diodes. *Advanced Functional Materials* **2016**, *26* (15), 2435−2445.

(2) Ravi, V. K.; Markad, G. B.; Nag, A. Band Edge Energies and Excitonic Transition Probabilities of Colloidal $CsPbX_3$ (X = Cl, Br, I) Perovskite Nanocrystals. *ACS Energy Letters* **2016**, *1* (4), 665−671.

(3) Kovalenko, M. V.; Protesescu, L.; Bodnarchuk, M. I. Properties and Potential Optoelectronic Applications of Lead Halide Perovskite Nanocrystals. *Science* **2017**, *358* (6364), 745−750.

(4) Lv, W.; Li, L.; Xu, M.; Hong, J.; Tang, X.; Xu, L.; Wu, Y.; Zhu, R.; Chen, R.; Huang, W. Improving the Stability of Metal Halide Perovskite Quantum Dots by Encapsulation. *Adv. Mater.* **2019**, *31* (28), No. 1900682.

(5) Wu, H.; Chen, Y.; Zhang, W.; Khan, M. S.; Chi, Y. Water-Dispersed Perovskite Nanocube@SiO_2-C_{18}-PC Core−Shell Nanoparticles for Cell Imaging. *ACS Applied Nano Materials* **2021**, *4* (11), 11791−11800.

(6) Yang, Z.; Xu, J.; Zong, S.; Xu, S.; Zhu, D.; Zhang, Y.; Chen, C.; Wang, C.; Wang, Z.; Cui, Y. Lead Halide Perovskite Nanocrystals-Phospholipid Micelles and Their Biological Applications: Multiplex Cellular Imaging and in Vitro Tumor Targeting. *ACS Appl Mater Interfaces* **2019**, *11* (51), 47671−47679.

(7) Wang, Y.; Varadi, L.; Trinchi, A.; Shen, J.; Zhu, Y.; Wei, G.; Li, C. Spray-Assisted Coil-Globule Transition for Scalable Preparation of Water-Resistant $CsPbBr_3$@PMMA Perovskite Nanospheres with Application in Live Cell Imaging. *Small* **2018**, *14* (51), No. 1803156.

(8) Lian, H.; Li, Y.; Saravanakumar, S.; Jiang, H.; Li, Z.; Wang, J.; Xu, L.; Zhao, W.; Han, G. Metal Halide Perovskite Quantum Dots for Amphiprotic Bio-Imaging. *Coord. Chem. Rev.* **2022**, *452*, No. 214313.

(9) Quan, L. N.; Rand, B. P.; Friend, R. H.; Mhaisalkar, S. G.; Lee, T. W.; Sargent, E. H. Perovskites for Next-Generation Optical Sources. *Chem Rev* **2019**, *119* (12), 7444−7477.

(10) Hu, T.; Li, D.; Shan, Q.; Dong, Y.; Xiang, H.; Choy, W. C. H.; Zeng, H. Defect Behaviors in Perovskite Light-Emitting Diodes. *ACS Materials Letters* **2021**, *3* (12), 1702−1728.

(11) Park, M.-H.; Kim, J. S.; Heo, J.-M.; Ahn, S.; Jeong, S.-H.; Lee, T.-W. Boosting Efficiency in Polycrystalline Metal Halide Perovskite Light-Emitting Diodes. *ACS Energy Letters* **2019**, *4* (5), 1134−1149.

(12) Dey, A.; Ye, J.; De, A.; Debroye, E.; Ha, S. K.; Bladt, E.; Kshirsagar, A. S.; Wang, Z.; Yin, J.; Wang, Y.; et al. State of the Art and Prospects for Halide Perovskite Nanocrystals. *ACS Nano* **2021**, *15* (7), 10775−10981.
(13) Shen, J.; Wang, Y.; Zhu, Y.; Gong, Y.; Li, C. A Polymer-Coated Template-Confinement $CsPbBr_3$ Perovskite Quantum Dot Composite. *Nanoscale* **2021**, *13* (13), 6586−6591.
(14) Xuan, T.; Yang, X.; Lou, S.; Huang, J.; Liu, Y.; Yu, J.; Li, H.; Wong, K. L.; Wang, C.; Wang, J. Highly Stable $CsPbBr_3$ Quantum Dots Coated with Alkyl Phosphate for White Light-Emitting Diodes. *Nanoscale* **2017**, *9* (40), 15286−15290.
(15) Tu, S.; Chen, M.; Wu, L. Dual-Encapsulation for Highly Stable All-Inorganic Perovskite Quantum Dots for Long-Term Storage and Reuse in White Light-Emitting Diodes. *Chemical Engineering Journal* **2021**, *412*, No. 128688.
(16) Li, Z.; Hofman, E.; Li, J.; Davis, A. H.; Tung, C.; Wu, L.; Zheng, W. Photoelectrochemically Active and Environmentally Stable $CsPbBr_3/TiO_2$ Core/Shell Nanocrystals. *Adv. Funct. Mater.* **2018**, *28* (1), No. 1704288.
(17) Pramata, A. D.; Akaishi, Y.; Kodama, N.; Mokuge, Y.; Kawashima, S.; Shimoyoshi, M.; Sairot, C.; Nuket, P.; Vas-Umnuay, P.; Kida, T. TiO_2-Coated $CsPbI_3$ Quantum Dots Coupled with Polyoxometalates for On/Off Fluorescent Photoswitches. *ACS Applied Nano Materials* **2021**, *4* (4), 4103−4113.
(18) Li, H.; Zhang, B.; Zhang, B.; Bala, H.; An, X.; Sha, N.; Sun, Z.; Zhang, W.; Zhang, Z. Core-Shell Structured $CsPbBr_3/Sn\text{-}TiO_2$ Nanocrystals for Visible-Light-Driven Photocatalyst in Aqueous Solution. *Appl. Surf. Sci.* **2022**, *599*, No. 153937.
(19) Loiudice, A.; Saris, S.; Oveisi, E.; Alexander, D. T. L.; Buonsanti, R. $CsPbBr_3$ QD/AlO_x Inorganic Nanocomposites with Exceptional Stability in Water, Light, and Heat. *Angew. Chem., Int. Ed. Engl.* **2017**, *56* (36), 10696−10701.
(20) Li, Z.; Kong, L.; Huang, S.; Li, L. Highly Luminescent and Ultrastable $CsPbBr_3$ Perovskite Quantum Dots Incorporated into a Silica/Alumina Monolith. *Angew. Chem., Int. Ed. Engl.* **2017**, *56* (28), 8134−8138.
(21) Zhou, W.; Zhao, Y.; Wang, E.; Li, Q.; Lou, S.; Wang, J.; Li, X.; Lian, Q.; Xie, Q.; Zhang, R. Q.; et al. Charge Transfer Boosting Moisture Resistance of Seminude Perovskite Nanocrystals via Hierarchical Alumina Modulation. *J Phys Chem Lett* **2020**, *11* (8), 3159−3165.
(22) Zhong, Q.; Cao, M.; Hu, H.; Yang, D.; Chen, M.; Li, P.; Wu, L.; Zhang, Q. One-Pot Synthesis of Highly Stable $CsPbBr_3$@SiO_2 Core-Shell Nanoparticles. *ACS Nano* **2018**, *12* (8), 8579−8587.
(23) Chen, D.; Fang, G.; Chen, X. Silica-Coated Mn-Doped $CsPb(Cl/Br)_3$ Inorganic Perovskite Quantum Dots: Exciton-to-Mn Energy Transfer and Blue-Excitable Solid-State Lighting. *ACS Appl Mater Interfaces* **2017**, *9* (46), 40477−40487.
(24) He, M.; Cheng, Y.; Shen, L.; Shen, C.; Zhang, H.; Xiang, W.; Liang, X. Mn-doped $CsPbCl_3$ Perovskite Quantum Dots (PQDs) Incorporated into Silica/Alumina Particles Used for WLEDs. *Appl. Surf. Sci.* **2018**, *448*, 400−406.
(25) Dirin, D. N.; Protesescu, L.; Trummer, D.; Kochetygov, I. V.; Yakunin, S.; Krumeich, F.; Stadie, N. P.; Kovalenko, M. V. Harnessing Defect-Tolerance at the Nanoscale: Highly Luminescent Lead Halide Perovskite Nanocrystals in Mesoporous Silica Matrixes. *Nano Lett* **2016**, *16* (9), 5866−5874.
(26) Zhang, H.; Wang, X.; Liao, Q.; Xu, Z.; Li, H.; Zheng, L.; Fu, H. Embedding Perovskite Nanocrystals into a Polymer Matrix for Tunable Luminescence Probes in Cell Imaging. *Adv. Funct. Mater.* **2017**, *27* (7), No. 1604382.
(27) Wei, Y.; Deng, X.; Xie, Z.; Cai, X.; Liang, S.; Ma, P.; Hou, Z.; Cheng, Z.; Lin, J. Enhancing the Stability of Perovskite Quantum Dots by Encapsulation in Crosslinked Polystyrene Beads via a Swelling−Shrinking Strategy toward Superior Water Resistance. *Adv. Funct. Mater.* **2017**, *27* (39), No. 1703535.
(28) Wang, Y.; Wang, S.; Yoo, J.; Yoon, D.; Li, T.; Wang, Y. Methylammonium Cation-Regulated Controllable Preparation of $CsPbBr_3$ Perovskite Quantum Dots in Polystyrene Fiber with Enhanced Water and UV Light Stabilities. *Inorg Chem* **2023**, *62* (22), 8626−8634.
(29) Cai, Y.; Zhang, P.; Bai, W.; Lu, L.; Wang, L.; Chen, X.; Xie, R.-J. Synthesizing Bright $CsPbBr_3$ Perovskite Nanocrystals with High Purification Yields and Their Composites with In Situ-Polymerized Styrene for Light-Emitting Diode Applications. *ACS Sustainable Chemistry & Engineering* **2022**, *10* (22), 7385−7393.
(30) Huang, Y.; Li, F.; Qiu, L.; Lin, F.; Lai, Z.; Wang, S.; Lin, L.; Zhu, Y.; Wang, Y.; Jiang, Y.; et al. Enhancing the Stability of $CH_3NH_3PbBr_3$ Nanoparticles Using Double Hydrophobic Shells of SiO_2 and Poly(vinylidene fluoride). *ACS Appl Mater Interfaces* **2019**, *11* (29), 26384−26391.
(31) Yu, Y.; Guo, J.; Bian, F.; Zhang, D.; Zhao, Y. Bioinspired Perovskite Quantum Dots Microfibers from Microfluidics. *Science China Materials* **2021**, *64* (11), 2858−2867.
(32) Yang, L.; Fu, B.; Li, X.; Chen, H.; Li, L. Poly(Vinylidene Fluoride)-Passivated $CsPbBr_3$ Perovskite Quantum Dots with Near-Unity Photoluminescence Quantum Yield and Superior Stability. *Journal of Materials Chemistry C* **2021**, *9* (6), 1983−1991.
(33) Wang, Z.; He, H.; Liu, S.; Wang, H.; Zeng, Q.; Liu, Z.; Xiong, Q.; Fan, H. J. Air Stable Organic-Inorganic Perovskite Nanocrystals@Polymer Nanofibers and Waveguide Lasing. *Small* **2020**, *16* (43), No. 2004409.
(34) Cha, W.; Kim, H.-J.; Lee, S.; Kim, J. Size-controllable and Stable Organometallic Halide Perovskite Quantum Dots/Polymer Films. *Journal of Materials Chemistry C* **2017**, *5* (27), 6667−6671.
(35) Liu, X. F.; Zou, L.; Yang, C.; Zhao, W.; Li, X. Y.; Sun, B.; Hu, C. X.; Yu, Y.; Wang, Q.; Zhao, Q.; et al. Fluorescence Lifetime-Tunable Water-Resistant Perovskite Quantum Dots for Multidimensional Encryption. *ACS Appl Mater Interfaces* **2020**, *12* (38), 43073−43082.
(36) Chen, L. C.; Tien, C. H.; Tseng, Z. L.; Dong, Y. S.; Yang, S. Influence of PMMA on All-Inorganic Halide Perovskite $CsPbBr_3$ Quantum Dots Combined with Polymer Matrix. *Materials (Basel)* **2019**, *12* (6), 985.
(37) Wang, B.; Peng, J.; Yang, X.; Cai, W.; Xiao, H.; Zhao, S.; Lin, Q.; Zang, Z. Template Assembled Large-Size $CsPbBr_3$ Nanocomposite Films toward Flexible, Stable, and High-Performance X-Ray Scintillators. *Laser Photoni. Rev.* **2022**, *16* (7), No. 2100736.
(38) Wu, D.; Chi, J.; Zhang, M.; Cheng, L.; Wang, X.; Fan, J.; Huang, Z.; Wang, H.; Xie, H.; Pan, Q.; Zhang, Z.; Chen, B.; Su, M.; Xu, B.; Song, Y.; et al. Water-Dispersing Perovskite Probes for the Rapid Imaging of Glioma Cells. *Adv. Opt. Mater.* **2022**, *10* (4), No. 2101835.
(39) Huynh, K. A.; Bae, S.-R.; Nguyen, T. V.; Do, H. H.; Heo, D. Y.; Park, J.; Lee, T.-W.; Le, Q. V.; Ahn, S. H.; Kim, S. Y. Ligand-Assisted Sulfide Surface Treatment of $CsPbI_3$ Perovskite Quantum Dots to Increase Photoluminescence and Recovery. *ACS Photonics* **2021**, *8* (7), 1979−1987.
(40) Huang, J.; Yang, H.; Chen, M.; Ji, T.; Hou, Z.; Wu, M. An Infrared Spectroscopy Study of PES PVP Blend and PES-g-PVP Copolymer. *Polymer Testing* **2017**, *59*, 212−219.
(41) Shen, X.; Zheng, J.; Meng, X.; Liang, Q. Fabrication and Magnetic Properties of Composite $Ni_{0.5}Zn_{0.5}Fe_2O_4/Pb(Zr_{0.52}Ti_{0.48})O_3$ Nanofibers by Electrospinning. *Journal of Wuhan University of Technology-Mater. Sci. Ed.* **2011**, *26* (3), 384−387.
(42) Loría-Bastarrachea, M. I.; Herrera-Kao, W.; Cauich-Rodríguez, J. V.; Cervantes-Uc, J. M.; Vázquez-Torres, H.; Ávila-Ortega, A. A TG/FTIR Study on the Thermal Degradation of Poly(Vinyl Pyrrolidone). *Journal of Thermal Analysis and Calorimetry* **2011**, *104* (2), 737−742.
(43) Devikala, S.; Ajith, D.; Kamaraj, P.; Arthanareeswari, M. Structural Morphological and Electrochemical Studies on PMMA/PVP Blends. *Materials Today: Proceedings* **2019**, *14*, 630−639.
(44) Yan, Q.-B.; Bao, N.; Ding, S.-N. Thermally Stable and Hydrophilic $CsPbBr_3$/mPEG-NH_2 Nanocrystals with Enhanced Aqueous Fluorescence for Cell Imaging. *Journal of Materials Chemistry B* **2019**, *7* (26), 4153−4160.

https://doi.org/10.1021/acsami.4c06854
ACS Appl. Mater. Interfaces 2024, 16, 34167−34180

(45) Li, S.; Lei, D.; Ren, W.; Guo, X.; Wu, S.; Zhu, Y.; Rogach, A. L.; Chhowalla, M.; Jen, A. K. Y. Water-Resistant Perovskite Nanodots Enable Robust Two-Photon Lasing in Aqueous Environment. *Nat. Commun.* **2020**, *11* (1), 1192.
(46) Kumar, P.; Patel, M.; Park, C.; Han, H.; Jeong, B.; Kang, H.; Patel, R.; Koh, W. G.; Park, C. Highly Luminescent Biocompatible $CsPbBr_3$@SiO_2 Core-Shell Nanoprobes for Bioimaging and Drug Delivery. *J Mater Chem B* **2020**, *8* (45), 10337−10345.
(47) Luo, F.; Li, S.; Cui, L.; Zu, Y.; Chen, Y.; Huang, D.; Weng, Z.; Lin, Z. Biocompatible Perovskite Quantum Dots with Superior Water Resistance Enable Long-Term Monitoring of the $H_{(2)}S$ Level in Vivo. *Nanoscale* **2021**, *13* (34), 14297−14303.
(48) Kar, M. R.; Chakraborty, R.; Patel, U.; Chakraborty, R.; Ray, S.; Acharya, T. K.; Goswami, C.; Bhaumik, S. Impact of Zn-Doping on the Composition, Stability, Luminescence Properties of Silica Coated All-Inorganic Cesium Lead Bromide Nanocrystals and their Biocompatibility. *Materials Today Chemistry* **2022**, *23*, No. 100753.
(49) Lou, S.; Zhou, Z.; Xuan, T.; Li, H.; Jiao, J.; Zhang, H.; Gautier, R.; Wang, J. Chemical Transformation of Lead Halide Perovskite into Insoluble, Less Cytotoxic, and Brightly Luminescent $CsPbBr_3$/$CsPb_2Br_5$ Composite Nanocrystals for Cell Imaging. *ACS Appl Mater Interfaces* **2019**, *11* (27), 24241−24246.
(50) Wang, J. X.; Liu, C.; Huang, H.; He, R.; Geng, S.; Yu, X. F. Microencapsulation of Lead-Halide Perovskites in an Oil-in-Fluorine Emulsion for Cell Imaging. *Nanomaterials (Basel)* **2023**, *13* (9), 1540.
(51) He, C.-L.; Meng, Z.-Q.; Ren, S.-X.; Li, J.; Wang, Y.; Wu, H.; Bu, H.; Zhang, Y.; Hao, W.-Z.; Chen, S.-L.; et al. Water-Ultrastable Perovskite $CsPbBr_3$ Nanocrystals for Fluorescence-Enhanced Cellular Imaging. *Rare Metals* **2023**, *42* (5), 1624−1634.
(52) Ryu, I.; Ryu, J.; Choe, G.; Kwon, H.; Park, H.; Cho, Y.; Du, R.; Yim, S. In Vivo Plain X-Ray Imaging of Cancer Using Perovskite Quantum Dot Scintillators. *Adv. Funct. Mater.* **2021**, *31* (34), No. 2102334.
(53) Zheng, J.; Zhang, W.; Huang, Y.; Shao, J.; Khan, M. S.; Chi, Y. Encapsulation of Pure Water-Stable Perovskite Nanocrystals (PNCs) into Biological Environment-Stable PNCs for Cell Imaging. *Inorg Chem* **2024**, *63* (12), 5623−5633.
(54) Li, M.; Tian, T.; Zeng, Y.; Zhu, S.; Lu, J.; Yang, J.; Li, C.; Yin, Y.; Li, G. Individual Cloud-Based Fingerprint Operation Platform for Latent Fingerprint Identification Using Perovskite Nanocrystals as Eikonogen. *ACS Appl Mater Interfaces* **2020**, *12* (11), 13494−13502.
(55) Jung, H. S.; Cho, J.; Neuman, K. C. Highly Stable Cesium Lead Bromide Perovskite Nanocrystals for Ultra-Sensitive and Selective Latent Fingerprint Detection. *Anal. Chim. Acta* **2021**, *1181*, No. 338850.
(56) Song, X.; Xu, Z.; Gao, B.; Li, X.; Lv, Q.; Zhang, R.; Wang, B.; Zhang, H.; Guo, P.; Ho, J. C. Red−Green−Blue Light Emission from Composition Tunable Semiconductor Micro-Tripods. *Adv. Funct. Mater.* **2024**, No. 2403135.
(57) Lee, H.; Park, J.; Kim, S.; Lee, S.; Kim, Y.; Lee, T. Perovskite Emitters as a Platform Material for Down-Conversion Applications. *Adv. Mater. Technol.* **2020**, *5* (10), No. 2000091.
(58) Zhou, Q.; Bai, Z.; Lu, W. G.; Wang, Y.; Zou, B.; Zhong, H. In Situ Fabrication of Halide Perovskite Nanocrystal-Embedded Polymer Composite Films with Enhanced Photoluminescence for Display Backlights. *Adv. Mater.* **2016**, *28* (41), 9163−9168.
(59) Sun, C.; Zhang, Y.; Ruan, C.; Yin, C.; Wang, X.; Wang, Y.; Yu, W. W. Efficient and Stable White LEDs with Silica-Coated Inorganic Perovskite Quantum Dots. *Adv. Mater.* **2016**, *28* (45), 10088−10094.
(60) Chen, W.; Shi, T.; Du, J.; Zang, Z.; Yao, Z.; Li, M.; Sun, K.; Hu, W.; Leng, Y.; Tang, X. Highly Stable Silica-Wrapped Mn-Doped $CsPbCl_3$ Quantum Dots for Bright White Light-Emitting Devices. *ACS Appl Mater Interfaces* **2018**, *10* (50), 43978−43986.
(61) Liu, H.; Wu, Z.; Shao, J.; Yao, D.; Gao, H.; Liu, Y.; Yu, W.; Zhang, H.; Yang, B. $CsPb_xMn_{1-x}Cl_3$ Perovskite Quantum Dots with High Mn Substitution Ratio. *ACS Nano* **2017**, *11* (2), 2239−2247.
(62) Yang, W.; Gao, F.; Qiu, Y.; Liu, W.; Xu, H.; Yang, L.; Liu, Y. $CsPbBr_3$-Quantum-Dots/Polystyrene@Silica Hybrid Microsphere Structures with Significantly Improved Stability for White LEDs. *Adv. Opt. Mater.* **2019**, *7* (13), No. 1900546.
(63) Jin, X.; Wang, C.; Miao, Y.; Liu, P.; Ji, J.; Chang, M.; Xu, B.; Zhao, M.; Tian, J.; Guo, J. In Situ Surface Reconstruction in Pure Water by Ice-Confined Freeze-Thaw Strategy for High-Performance Core−Shell Structural Perovskite Nanocrystals. *Adv. Funct. Mater.* **2024**, No. 2401435.
(64) Gao, F.; Yang, W.; Liu, X.; Li, Y.; Liu, W.; Xu, H.; Liu, Y. Highly Stable and Luminescent Silica-Coated Perovskite Quantum Dots at Nanoscale-Particle Level via Nonpolar Solvent Synthesis. *Chemical Engineering Journal* **2021**, *407*, No. 128001.
(65) Park, J.; Jang, K. Y.; Lee, S. H.; Kim, D.-H.; Cho, S.-H.; Lee, T.-W. Stable Orthorhombic $CsPbBr_3$ Light Emitters: Encapsulation-Assisted In Situ Synthesis. *Chem. Mater.* **2023**, *35* (16), 6266−6273.
(66) Yuan, L.; Zhou, Y.; Wang, Z.; Mei, E.; Liang, X.; Xiang, W. Eco-Friendly All-Inorganic $CsPbX_3$ (X = Cl, Br, and I) Perovskite Nanocrystals in Pyrophyllite for Bright White Light-Emitting Diodes. *Applied Clay Science* **2021**, *211*, No. 106158.
(67) Guan, H.; Zhao, S.; Wang, H.; Yan, D.; Wang, M.; Zang, Z. Room Temperature Synthesis of Stable Single Silica-Coated $CsPbBr_3$ Quantum Dots Combining Tunable Red Emission of Ag−In−Zn−S for High-CRI White Light-Emitting Diodes. *Nano Energy* **2020**, *67*, No. 104279.
(68) Mo, Q.; Chen, C.; Cai, W.; Zhao, S.; Yan, D.; Zang, Z. Room Temperature Synthesis of Stable Zirconia-Coated $CsPbBr_3$ Nanocrystals for White Light-Emitting Diodes and Visible Light Communication. *Laser Photon. Rev.* **2021**, *15* (10), No. 2100278.
(69) Yan, D.; Zhao, S.; Zhang, Y.; Wang, H.; Zang, Z. Highly Efficient Emission and High-CRI Warm White Light-Emitting Diodes from Ligand-Modified $CsPbBr_3$ Quantum Dots. *Opto-Electronic Advances* **2022**, *5* (1), No. 200075.
(70) Li, X.; Ma, W.; Liang, D.; Cai, W.; Zhao, S.; Zang, Z. High-Performance $CsPbBr_3$@Cs_4PbBr_6/SiO_2 Nanocrystals via Double Coating Layers for White Light Emission and Visible Light Communication. *eScience* **2022**, *2* (6), 646−654.

https://doi.org/10.1021/acsami.4c06854
ACS Appl. Mater. Interfaces 2024, 16, 34167−34180